



## ARTICLE

## tRF3-IleAAT reduced extracellular matrix synthesis in diabetic kidney disease mice by targeting ZNF281 and inhibiting ferroptosis

Yun-yang Qiao<sup>1,2</sup>, Jia-ling Ji<sup>2</sup>, Wei-ling Hou<sup>3</sup>, Gao-ting Qu<sup>1</sup>, Shan-wen Li<sup>1</sup>, Xing-yue Li<sup>1</sup>, Ran Jin<sup>1</sup>, Yin-fang Li<sup>1</sup>, Hui-min Shi<sup>1</sup>✉ and Ai-qing Zhang<sup>2</sup>✉

It is well established that the synthesis of extracellular matrix (ECM) in mesangial cells is a major determinant of diabetic kidney disease (DKD). Elucidating the major players in ECM synthesis may be helpful to provide promising candidates for protecting against DKD progression. tRF3-IleAAT is a tRNA-derived fragment (tRF) produced by nucleases at tRNA-specific sites, which is differentially expressed in the sera of patients with diabetes mellitus and DKD. In this study we investigated the potential roles of tRFs in DKD. *Db/db* mice at 12 weeks were adapted as a DKD model. The mice displayed marked renal dysfunction accompanied by significantly reduced expression of tRF3-IleAAT and increased ferroptosis and ECM synthesis in the kidney tissues. The reduced expression of tRF3-IleAAT was also observed in high glucose-treated mouse glomerular mesangial cells. We administered ferrostatin-1 (1 mg/kg, once every two days, i.p.) to the mice from the age of 12 weeks for 8 weeks, and found that inhibition of the onset of ferroptosis significantly improved renal function, attenuated renal fibrosis and reduced collagen deposition. Overexpression of tRF3-IleAAT by a single injection of AAV carrying tRF3-IleAAT via caudal vein significantly inhibited ferroptosis and ECM synthesis in DKD model mice. Furthermore, we found that the expression of zinc finger protein 281 (ZNF281), a downstream target gene of tRF3-IleAAT, was significantly elevated in DKD models but negatively regulated by tRF3-IleAAT. In high glucose-treated mesangial cells, knockdown of ZNF281 exerted an inhibitory effect on ferroptosis and ECM synthesis. We demonstrated the targeted binding of tRF3-IleAAT to the 3'UTR of ZNF281. In conclusion, tRF3-IleAAT inhibits ferroptosis by targeting ZNF281, resulting in the mitigation of ECM synthesis in DKD models, suggesting that tRF3-IleAAT may be an attractive therapeutic target for DKD.

**Keywords:** diabetic kidney disease; extracellular matrix; ferroptosis; tRNA-derived fragments; Zinc finger protein 281; ferrostatin-1

*Acta Pharmacologica Sinica* (2024) 0:1–12; <https://doi.org/10.1038/s41401-024-01228-5>

## INTRODUCTION

Diabetic kidney disease (DKD), which is characterized by massive proteinuria and a reduced glomerular filtration rate, is among the most common complications of diabetes mellitus and has become a global public health problem [1]. DKD is also a major cause of end-stage renal disease in most developed countries [2]. Increasing evidence reveals that renal fibrosis is a recognized pathological pathway of DKD [3, 4]. The pathological basis of DKD involves thickening of the basement membrane, hypertrophy of glomeruli, deposition of multiple extracellular matrix (ECM) components, and proliferation and hypertrophy of mesangial cells, which are important fibroblasts [5, 6]. Mesangial cells are important fibrotic effector cells that can be abnormally activated and proliferate early in the development of DKD, promoting ECM synthesis, which is a key factor leading to pathological changes in DKD [7, 8].

tRNA-derived fragments (tRFs) are a class of small noncoding RNAs produced by specific nucleases that cleave at specific sites

on the tRNA loop [9–11]. tRFs function in numerous diseases, including tumors, infections and neurological disorders, due to their high degree of conservation and stability [12–14]. The development of next-generation sequencing technology has led to many significant discoveries. A series of differentially expressed tRFs have been identified in transforming growth factor-1-treated mesangial cells as well as renal podocytes during growth, differentiation and injury [15, 16]; thus, tRFs may have an important regulatory role in the development of chronic kidney disease. In our previous study, six differentially expressed tRFs were screened by high-throughput sequencing of sera from patients with diabetes and DKD, suggesting that tRFs may play an important regulatory role in DKD [17]. However, the specific mechanism of tRFs in the pathogenesis of DKD remains unclear.

Ferroptosis is a novel iron-dependent form of programmed cell death characterized by increased production of reactive oxygen species (ROS) and mitochondrial alterations accompanied by

<sup>1</sup>Department of Pediatric Nephrology, the Second Affiliated Hospital of Nanjing Medical University, Nanjing 210003, China; <sup>2</sup>Department of Pediatrics, the Fourth Affiliated Hospital of Nanjing Medical University, Nanjing 210031, China and <sup>3</sup>Department of Science and Education, the Affiliated Jiangning Hospital of Nanjing Medical University, Nanjing 211199, China

Correspondence: Hui-min Shi (shihuimin@njmu.edu.cn) or Ai-qing Zhang (njqaiqing@njmu.edu.cn)

These authors contributed equally: Yun-yang Qiao, Jia-ling Ji

Received: 26 August 2023 Accepted: 11 January 2024

numerous genetic and protein changes [18]. Glutathione peroxidase 4 (GPX4) plays a crucial role as an antioxidant. GPX4 activity is activated by glutathione (GSH), which is produced by solute carrier family 7 member 11 (SLC7A11); when the antioxidant system is destabilized, GSH production is affected, and the regulatory core enzyme GPX4 is further reduced and loses its antioxidant capacity [19, 20]. Thus, a unique form of cell death characterized by low GSH levels and high lipid peroxidation occurs. Polyunsaturated fatty acids are important targets of lipid peroxidation, and their binding to phospholipids is a vital contributor. This binding is functionally dependent on the involvement of acyl-CoA synthetase long-chain family member 4 (ACSL4); activation of ACSL4 drives the production of lipid oxides by the iron-containing enzyme lipoxygenase, which further promotes ferroptosis [21]. Although ferroptosis was initially found in cancer cells, an increasing number of studies have indicated that ferroptosis plays important roles in renal diseases [22–24].

The role of tRFs in DKD, which involves the regulation of ferroptosis, remains elusive. To explore the potential functions of tRFs in DKD, we studied tRF3-IleAAT, which is significantly downregulated in the sera of DKD patients, in *db/db* mice and high glucose (HG)-induced mesangial cells. The downstream effects were assessed using an adeno-associated virus (AAV) and a mimetic for overexpression of tRF3-IleAAT. In this study, we identified zinc finger protein 281 (ZNF281) as a downstream target of tRF3-IleAAT and explored the mechanism of action. Elucidating the role and mechanism of tRF3-IleAAT in regulating ECM synthesis in DKD will provide a basis and rationale for the clinical application in DKD.

## MATERIALS AND METHODS

### Animal model and therapeutic experiments

Eight-week-old male *db/m* and *db/db* mice were used in the in vivo experiments and were purchased from GemPharmatech LLC (Nanjing, China). All experiments were conducted after approval by the Experimental Animal Welfare Ethics Committee of Nanjing Medical University (No. IACUC-2206034) and conformed with the Helsinki Declaration. Every effort was made to minimize animal suffering during the experiments, which were performed in strict accordance with the “Guidelines for the Care and Use of Laboratory Animals”. Blood glucose, body weight, urine volume and urine protein were measured at necessary time points. The DKD model was successfully established at 12 weeks, and AAV interventions, as well as corresponding negative control (NC) (GeneChem, Shanghai, China) and ferrostatin-1 (Fer-1) (MCE, Monmouth Junction, NJ, USA) interventions, were performed [25]. Overall, mice were divided into the following groups ( $n=6$  per group): (1) the *db/m* group, (2) the *db/db* group, (3) the *db/db* + AAV tRF3-IleAAT group, (4) the *db/db* + AAV tRF-NC group, (5) the *db/db*+Fer-1 group, and (6) the *db/m*+Fer-1 group. *Db/db* + AAV tRF3-IleAAT and *db/db* + AAV tRF-NC mice were administered a single injection of  $1 \times 10^{12}$  particles of AAV carrying tRF3-IleAAT or tRF3-IleAAT NC via the caudal vein. Starting at 12 weeks of age, *db/m*+Fer-1 and *db/db*+Fer-1 mice were injected intraperitoneally with Fer-1 at 1 mg/kg once every two days for 8 weeks. Fer-1 was dissolved in dimethyl sulfoxide (DMSO) (MCE, Monmouth Junction, NJ, USA) and further diluted with a final concentration of DMSO not exceeding 0.1%. Mice were anesthetized with sodium barbiturate (100 mg/kg) at 20 weeks of age and sacrificed, and further samples were collected for subsequent experiments.

### Cell lines and culture conditions

Mouse glomerular mesangial cells (SV40-MES 13) (CL-0470, Lot: BXO5T8YYYI) were purchased from Procell Life Sciences & Technology Co. (Wuhan, China) and were cultured and acclimated in normal glucose (5.5 mM) Dulbecco's modified Eagle's medium

(DMEM) (Gibco, Rockville, MD, USA) containing 10% fetal bovine serum (FBS) (Gibco, Rockville, MD, USA). Cells were cultured in DMEM containing 10% FBS with the addition of glucose to establish an HG group (30 mM), while a mannitol group (5.5 mM + 24.5 mM) was set up to exclude the effect of high osmolality of HG on the cells.

### Cell transfection

The tRF3-IleAAT mimetic, ZNF281 small interfering RNA (siRNA) and respective NCs were purchased from RiboBio (Guangzhou, China). ZNF281 plasmids were constructed by RiboBio to allow for overexpression. Cells were inoculated into 6-well or 12-well plates the day before transfection, and when the cell density reached 50%, transfections were performed with a RiboFect CP Transfection Kit (RiboBio, Guangzhou, China). Transfection mixtures were prepared using specific buffer and reagent to a final concentration of 20 nM, with appropriate experimental interventions. Real-time quantitative polymerase chain reaction (RT-qPCR) and Western blotting were performed to measure transfection efficiency. The sequences of tRF3-IleAAT and ZNF281 for transfection are listed in Supplementary Table S1.

### RT-qPCR

Total RNA was extracted from kidney tissues or cells by using TRIzol reagent (Invitrogen, CA, USA). For tRF3-IleAAT, 1000 ng of total RNA was reverse-transcribed (Vazyme, Nanjing, China). Subsequently, RT-qPCR for tRF3-IleAAT was performed, and the expression levels were normalized to that of U6. To measure mRNA, cDNA synthesis and subsequent RT-qPCR were performed using HScript III RT SuperMix (Vazyme, Nanjing, China) and ChamQ Universal SYBR qPCR Master Mix (Vazyme, Nanjing, China), respectively.  $\beta$ -Actin was used as an internal control for normalization. All mRNA primers were purchased from GeneRay Biotech Co., Ltd. (Shanghai, China); the sequences are listed in Supplementary Table S2.

### Western blotting

Total protein from kidney tissues and mesangial cells was extracted with lysis buffer (Beyotime, Shanghai, China). The suspensions were collected and lysed on ice and then centrifuged at  $12,000 \times g$  at 4 °C for 30 min. The protein concentrations were measured with a bicinchoninic acid protein assay kit (Beyotime, Shanghai, China). After quantification, 50  $\mu$ g of total protein was loaded and separated by electrophoresis and subsequently transferred to a polyvinylidene fluoride membrane (Millipore, Boston, MA, USA). After blocking, the membranes were immersed in primary antibody and incubated overnight at 4 °C. The following day, the membranes were incubated with the secondary antibody and washed, after which the protein bands were exposed. Immunoblot analysis was performed with the following primary antibodies: anti-fibronectin (FN) (1:1000, ab2413, Abcam, Cambridge, UK), anti-collagen I (Col I) (1:500, sc-59772, Santa Cruz, Dallas, Texas, USA), anti-GPX4 (1:1000, ab125066, Abcam, Cambridge, UK), anti-SLC7A11 (1:1000, ab175186, Abcam, Cambridge, UK), anti-ACSL4 (1:500, sc-365230, Santa Cruz, Dallas, Texas, USA), and anti-ZNF281 (1:1000, PAB37901, Bioswamp, Wuhan, China). The secondary antibodies were horseradish peroxidase-conjugated goat anti-rabbit and goat anti-mouse antibodies purchased from Abbkine (1:10000, Wuhan, China).  $\beta$ -Tubulin (1:1000, AF7011, Affinity biosciences, Changzhou, China) was served as an internal control.

### Serum creatinine (sCr) and 24 h urine protein quantification

Collected mouse blood and urine samples were centrifuged, and the supernatant was obtained for further assays. Assays were performed according to the kit instructions (Jiancheng, Nanjing, China). Blood samples were spiked into 96-well plates, including standard wells, blank wells and assay wells, and incubated at 37 °C

for 5 min. The absorbance values of all wells were measured at 546 nm, and the sCr content ( $\mu\text{mol/L}$ ) of each sample was calculated according to the formula in the instructions. For measurement of urine protein, 5 $\times$  reagent was diluted for use, and the samples were added sequentially to a 96-well plate. The samples were mixed thoroughly and left to stand for several minutes after addition. The absorbance values of all wells were measured at 595 nm. The urine protein concentration ( $\text{mg/L}$ ) was obtained according to the calculation formula provided, and the 24 h urine protein value was further calculated based on the 24 h urine volume of mice corresponding to the samples.

#### Immunofluorescence and immunohistochemistry

Three-micrometer-thick paraffin-embedded renal tissue sections were prepared. The sections were baked, dewaxed, hydrated and then blocked with 5% bovine serum albumin for 2 h. Subsequent operations were performed according to the manufacturer's instructions (Maixin, Fuzhou, China). The tissue sections were incubated with primary antibodies against FN and ZNF281, and the nuclei were stained and sealed after secondary antibody incubation. The immunostained samples were observed, and images were obtained under a confocal microscope (FV1000, Olympus).

#### Malondialdehyde (MDA) assay

MDA contents were measured to assess lipid peroxidation levels by using an MDA microassay kit purchased from Abbkine (Wuhan, China). A total of  $5 \times 10^6$  cells were collected, and 1 mL of precooled extraction buffer was added. Ultrasonic cell disruption was performed, and the disrupted cells were centrifuged at  $13,000 \times g$  for 10 min at 4 °C. The supernatant was collected, and the working reagent was configured as needed. The samples were incubated in a water bath at 95 °C for 30 min and then centrifuged at  $10,000 \times g$  for 10 min at room temperature. The supernatant was added to a 96-well plate, and the absorbance values of each well at 532 nm and 600 nm were measured to further calculate the MDA content of each well.

#### GSH assay

GSH was used to assist in determining the cellular redox status. Cell or tissue samples were collected and added to precooled extraction buffer. After the samples were lysed, they were centrifuged, and the supernatant was placed on ice. A 200  $\mu\text{g/mL}$  GSH standard was prepared, and standard wells, blank wells and assay wells were set up in a 96-well plate according to the instruction manual of the kit. The samples were added, and the absorbance values at 412 nm were measured. A standard curve was plotted to calculate the GSH content of the assay wells.

#### Ferrous ion ( $\text{Fe}^{2+}$ ) assay

An  $\text{Fe}^{2+}$  assay was performed according to the manufacturer's instructions (Elabscience, Wuhan, China). Approximately  $1 \times 10^6$  cells were collected, and 0.2 mL of buffer was added and mixed well. The cells were lysed on ice and then centrifuged at  $15,000 \times g$  for 15 min. The supernatant was obtained and set aside. A standard of 100  $\mu\text{mol/L}$  was prepared and added to the standard wells at different concentrations. The samples were then added to the control and assay wells in order, mixed and incubated. The absorbance values of all wells were measured at 593 nm, and the  $\text{Fe}^{2+}$  concentration of each sample was calculated.

#### ROS assay

In situ loading of ROS levels was performed using a fluorescent probe (Beyotime, Shanghai, China). After a negative reference was set and the optimal probe concentration for the cells was explored, the probe was diluted with serum-free culture medium at 1:2000 to a final concentration of 5  $\mu\text{mol/L}$ . After the cell culture

medium was removed, the probe was added to cover the cells, and the cells were incubated in a 37 °C cell culture incubator for 40 min with shaking. The cells were washed and resuspended in phosphate-buffered saline, and cellular ROS levels were assessed by flow cytometry.

#### Masson staining

Tissue wax blocks were sliced to a thickness of 3  $\mu\text{m}$ , and the samples were baked in an oven overnight. The sections were soaked in xylene and different concentrations of alcohol in a fume hood and washed with ddH<sub>2</sub>O. Using a Masson staining kit (Servicebio, Wuhan, China), the sections were sequentially dipped in Masson solution. The sections were subsequently rinsed and separated with 1% glacial acetic acid and sealed with neutral gum after being soaked in anhydrous ethanol and xylene. Finally, microscopic examination was performed, and images were collected for analysis.

#### Dual-luciferase reporter assay

As ZNF281 was a predicted target gene of trf3-IleAAT, the ZNF281 mRNA 3'UTR sequence was chemically synthesized, and both wild-type (WT) ZNF281 and mutant (MUT) ZNF281 plasmids were constructed by RiboBio. When the cell density reached 50%, Lipofectamine 2000 was used to cotransfect the luciferase reporter plasmid, trf3-IleAAT mimetic and trf-IleAAT NC into mesangial cells. The cells were collected and lysed, and luciferase activity was assayed using a dual-luciferase reporter kit (GenePharma, Shanghai, China). The data were then analysed.

#### Statistical analysis

All measurement data are presented as the mean  $\pm$  standard deviation (SD) from three independent experiments. Statistical analysis was performed with GraphPad Prism 8.0.1 (GraphPad Software, Inc.). Unpaired Student's *t* test was used for two-group comparisons, and one-way analysis of variance was used for comparisons among multiple groups. *P* < 0.05 was considered to indicate statistical significance.

## RESULTS

trf3-IleAAT is downregulated in DKD models

Our previous sequencing results showed that trf3-IleAAT expression was significantly reduced in sera from patients with DKD, and further functional analysis indicated that cell death and energy metabolism were associated with trf3-IleAAT [17]. Here, the downregulation of trf3-IleAAT in *db/db* mice was first verified (Fig. 1a). In addition, the 24 h urine protein and sCr levels of all mice were measured at 20 weeks of age, and those of *db/db* mice were found to be significantly higher than those of *db/m* mice (Fig. 1b). Light microscopy was used to examine the histopathological morphology of kidneys at 20 weeks of age. The *db/db* group had kidneys with an abnormal histopathological morphology as well as increased and significantly dilated glomerular mesangial stroma, interstitial collagen deposition and increased fibrosis (Fig. 1c and Supplementary Fig. S1a). Moreover, in the glomeruli of *db/db* mice, the fluorescence of the ECM component FN was significantly enhanced (Fig. 1d). The results showed that the expression of FN and Col I, which are related to ECM synthesis, was significantly higher in the *db/db* group than in the *db/m* group (Fig. 1e, f and Supplementary Fig. S1b). Mouse glomerular mesangial cells were cultured and treated with HG (30 mM) in vitro for 24 h. The low expression levels of trf3-IleAAT were verified by RT-qPCR (Fig. 1g). FN and Col I were measured by RT-qPCR and Western blotting and the results showed that the expression was significantly higher in the HG group than in the control group, but there was no significant change in the mannitol group (Fig. 1h, i and Supplementary Fig. S1c), suggesting that high osmotic pressure did not significantly affect ECM synthesis.



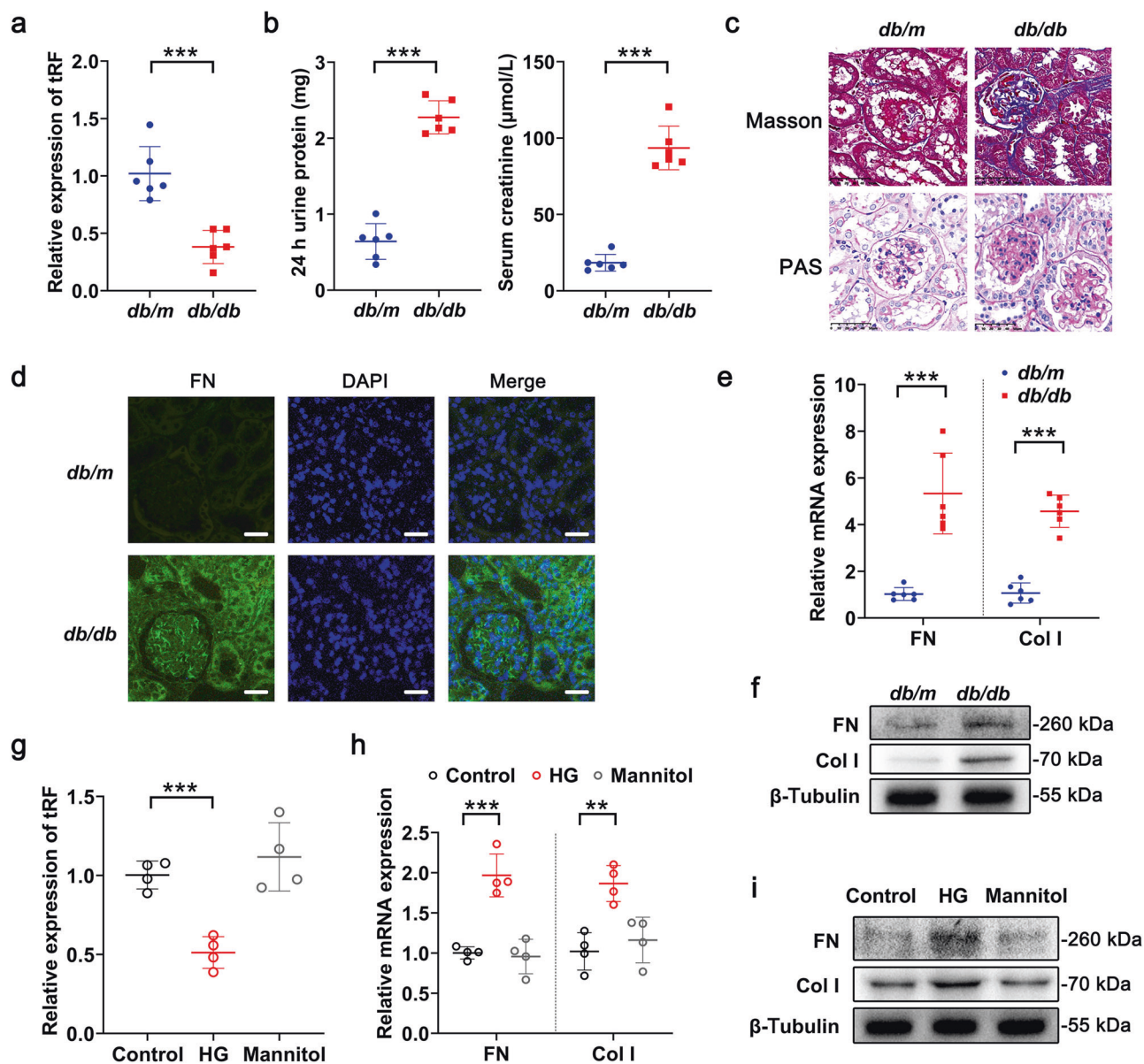


**Fig. 1** tRF3-IleAAT is downregulated in DKD models. **a** tRF3-IleAAT was validated by RT-qPCR in *db/db* mice, with U6 as a normalization control. **b** 24 h urine protein and sCr levels in mice at 20 weeks of age. **c** Representative images of Masson and PAS staining of glomeruli in the renal cortex. Scale bar, 50  $\mu\text{m}$ . **d** Representative images of immunofluorescence of FN in the kidney tissues of mice. Scale bar, 20  $\mu\text{m}$ . **e**, **f** The expression levels of FN and Col I in the kidney tissues of mice were measured by RT-qPCR and Western blotting. **g** tRF3-IleAAT expression was measured by RT-qPCR in HG-induced mesangial cells, with U6 as a normalization control. **h**, **i** Expression of FN and Col I in HG-treated mesangial cells. The data are expressed as the mean  $\pm$  SD. \*\* $P < 0.01$ , \*\*\* $P < 0.001$  vs. the indicated group.

tRF3-IleAAT overexpression alleviates ECM synthesis in DKD models

Considering that the downregulation of tRF3-IleAAT is associated with the synthesis of ECM in DKD models, we hypothesized that tRF3-IleAAT may have a therapeutic effect in DKD. The significant increases in body weight, blood glucose, urine volume and 24 h urine protein levels in *db/db* mice at 12 weeks of age suggested that the model was successfully established (Supplementary Fig. S2a, b). We overexpressed tRF3-IleAAT by injecting AAV into the tail vein and established a corresponding NC group. At 20 weeks of age, the tRF3-IleAAT expression levels in kidney tissues from the *db/db* + AAV tRF3-IleAAT group were significantly higher, suggesting successful overexpression (Fig. 2a).

We further assessed the role of tRF3-IleAAT in the synthesis of ECM in *db/db* mice. For examination of renal function, 24 h urine protein and

sCr levels were examined, and the results showed that mice in the *db/db* + AAV tRF3-IleAAT group exhibited somewhat reduced sCr and 24 h urine protein levels (Fig. 2b). We tracked the changes in body weight and blood glucose in each group of mice; however, there were no significant differences between the *db/db* + AAV tRF-NC and *db/db* + AAV tRF3-IleAAT groups (Supplementary Fig. S2b). Histopathologically, Masson staining showed that the area of collagen deposition was reduced in the *db/db* + AAV tRF3-IleAAT group compared with the *db/db* + AAV tRF-NC group; in combination with periodic acid-Schiff (PAS) staining, this finding indicated reduced glomerular dilatation and fibrosis (Fig. 2c and Supplementary Fig. S2c). Immunofluorescence showed diminished FN fluorescence intensity in the *db/db* + AAV tRF3-IleAAT group (Fig. 2d). RT-qPCR and Western blotting were performed to measure the expression levels of FN and Col I and the results showed that the mRNA and protein levels were significantly lower in

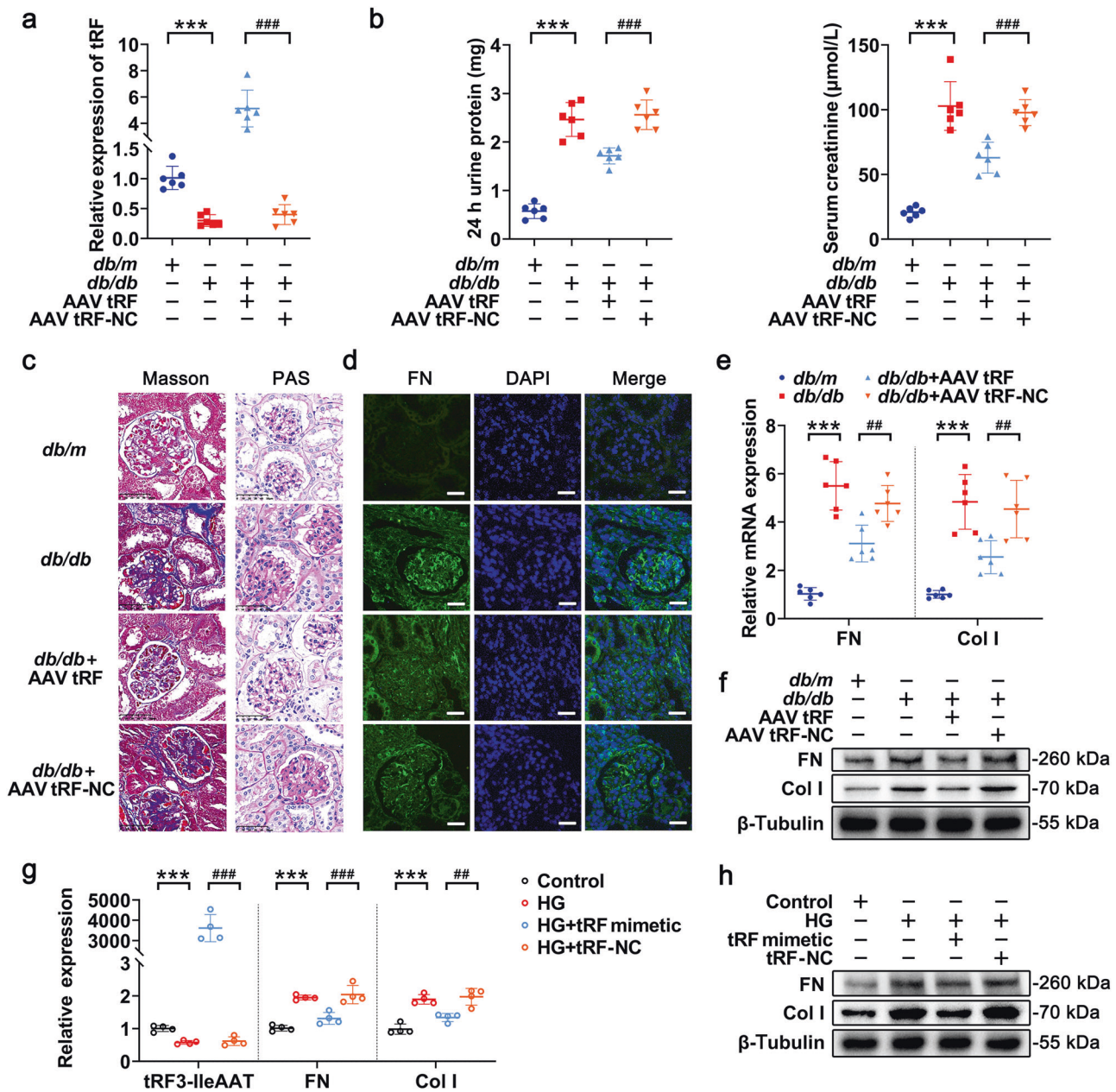


**Fig. 2** tRF3-IleAAT overexpression alleviates ECM synthesis in DKD models. **a** In vivo experiments were performed to overexpress tRF3-IleAAT and verify the expression levels by RT-qPCR, with U6 as a normalization control. **b** 24 h urine protein and sCr levels in each group of mice. **c** Representative images of Masson and PAS staining presenting the improvement in glomerular morphology mediated by tRF3-IleAAT, including the reduction in matrix deposition. Scale bar, 50 μm. **d** Fluorescence intensity of FN in each group of glomeruli. Scale bar, 20 μm. **e, f** RT-qPCR and Western blot analysis of FN and Col I in each group of mice. **g, h** Overexpression of tRF3-IleAAT in HG-treated mesangial cells and verification of the expression levels by RT-qPCR and Western blot. Expression of FN and Col I after tRF3-IleAAT mimetic treatment in HG-treated mesangial cells. The data are expressed as the mean ± SD. \*\*\**P* < 0.001, \*\**P* < 0.01, ###*P* < 0.001 vs. the indicated group.

the *db/db* + AAV tRF3-IleAAT group than in the *db/db* + AAV tRF-NC group (Fig. 2e, f and Supplementary Fig. S2d). To clarify the effect of tRF3-IleAAT on ECM synthesis, tRF3-IleAAT was overexpressed in vitro by using the tRF mimetic method, and its overexpression was verified by RT-qPCR. The results showed that the expression of tRF3-IleAAT in the HG+tRF3-IleAAT mimetic group was significantly higher, suggesting successful overexpression (Fig. 2g). On this basis, we further identified the role of tRF3-IleAAT in ECM synthesis. The results showed that the mRNA and protein expression levels of FN and Col I were significantly lower in the HG+tRF3-IleAAT mimetic group than in the HG+tRF3-IleAAT NC group (Fig. 2g, h and Supplementary Fig. S2e).

Inhibition of ferroptosis alleviates ECM synthesis in vivo and in vitro

In our previous study, the Kyoto Encyclopedia of Genes and Genomes suggested that tRF3-IleAAT may be closely associated with cell death and lipid metabolism, and its function is highly enriched in ferroptosis-related signaling pathways [17]. Here, to investigate the role of ferroptosis in DKD, the expression levels of ferroptosis-related indicators were measured by RT-qPCR and Western blotting in mice. The results showed that the expression of ACSL4 was significantly higher, while those of GPX4 and SLC7A11 were significantly lower, in the kidney tissues of mice from the



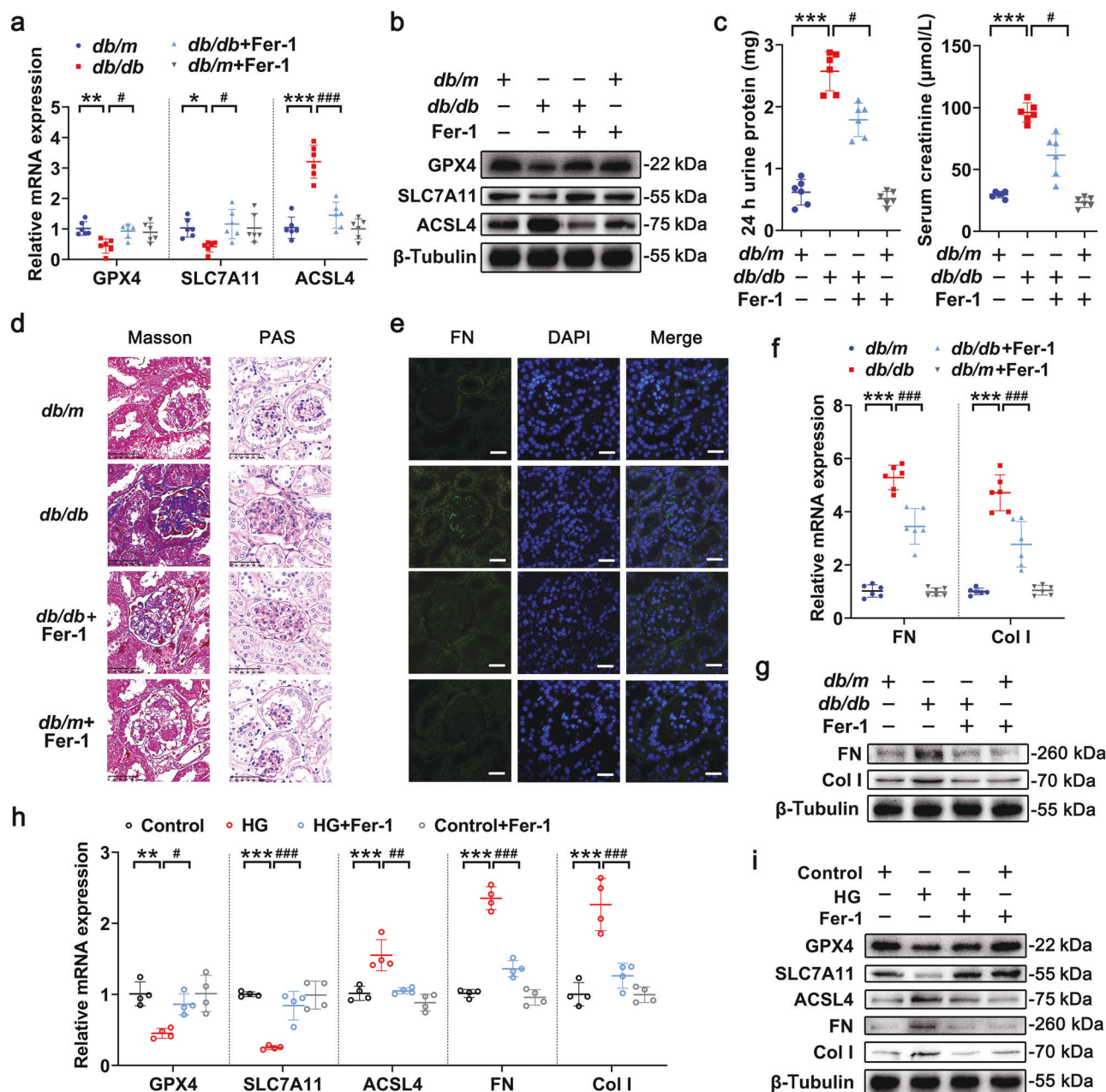


**Fig. 3** Inhibition of ferroptosis alleviates ECM synthesis in vivo and in vitro. **a, b** RT-qPCR and Western blotting were used to measure the expression levels of ferroptosis-related indicators in the kidney tissues of *db/db* mice. **c** 24 h urine protein and sCr levels in mice. **d** Masson and PAS staining were performed to examine alterations in glomerular pathological morphology by Fer-1. Scale bar, 50  $\mu$ m. **e** The intensity of FN in the glomerulus was observed by immunofluorescence. Scale bar, 20  $\mu$ m. **f, g** The expression levels of ECM-related indicators were analysed by RT-qPCR and Western blotting. **h, i** The levels of ferroptosis-related indicators were measured by RT-qPCR and Western blotting in HG-induced mesangial cells to verify the role of Fer-1. RT-qPCR and Western blot analysis of FN and Col I were performed to assess the effect of ferroptosis on ECM synthesis. The data are expressed as the mean  $\pm$  SD. \* $P$  < 0.05, \*\* $P$  < 0.01, \*\*\* $P$  < 0.001, # $P$  < 0.05, ## $P$  < 0.01, ### $P$  < 0.001 vs. the indicated group.

*db/db* group than in the *db/m* group (Fig. 3a, b and Supplementary Fig. S3a), corroborating that ferroptosis occurred. Previous studies have shown that Fer-1 is a potent and selective inhibitor of ferroptosis, so we observed the effect of ferroptosis on renal function and ECM synthesis via intraperitoneal injection of Fer-1 in *db/db* mice [18, 26]. RT-qPCR and Western blotting revealed significantly lower ACSL4 expression and significantly higher GPX4 and SLC7A11 expression in the *db/db+Fer-1* group than in the *db/db* group (Fig. 3a, b and Supplementary Fig. S3a). We focused on the key question of how renal fibrosis, including ECM synthesis, is affected in *db/db* mice after ferroptosis is inhibited. We were

surprised to find that the 24 h urine protein and sCr levels were significantly lower in the *db/db+Fer-1* group of mice (Fig. 3c). Regarding histopathology, the mice in the *db/db+Fer-1* group showed reduced collagen deposition, lower levels of glomerular expansion and less fibrosis (Fig. 3d and Supplementary Fig. S3b). Further immunofluorescence showed that the fluorescence intensity of FN was diminished in the *db/db+Fer-1* group (Fig. 3e). Moreover, RT-qPCR showed that the expression levels of renal FN and Col I were significantly lower in the *db/db+Fer-1* group than in the *db/db* group (Fig. 3f). The Western blotting and RT-qPCR results were consistent (Fig. 3g and Supplementary Fig. S3c).

In cellular experiments, RT-qPCR and Western blotting results showed that the ferroptosis-related expression levels were significantly changed in the HG group than in the control group (Supplementary Fig. S3d, e). Moreover, the  $\text{Fe}^{2+}$  contents and MDA levels were significantly elevated in the HG group, and GSH levels showed a decreasing trend compared with those in the control group (Supplementary Fig. S3f–h). Flow cytometry analysis also showed that ROS levels were significantly elevated in the HG group (Supplementary Fig. S3i). We further examined the causal relationship between the synthesis of renal ECM and ferroptosis in cells. The changes in the expression levels of ferroptosis-related indicators were reversed in the HG+Fer-1 group compared with the HG group, again demonstrating the inhibitory effect of Fer-1 on ferroptosis (Fig. 3h, i and Supplementary Fig. S3j). The MDA contents and GSH levels were also altered in the HG+Fer-1 group, further clarifying the role of Fer-1 (Supplementary Fig. S3k, l). The expression levels of FN and Col I were examined to clarify the effect of ferroptosis on ECM synthesis, and the expression was significantly lower in the HG+Fer-1 group than in the HG group (Fig. 3h, i and Supplementary Fig. S3j). Cellular experiments verified that ferroptosis is a key factor in ECM synthesis.

**tRF3-IleAAT overexpression alleviates ferroptosis in DKD models**  
Overexpression of tRF3-IleAAT and inhibition of ferroptosis are known to reduce ECM synthesis in DKD. Here, we hypothesized that tRF3-IleAAT may inhibit ferroptosis to reduce ECM synthesis. The role of tRF3-IleAAT in the onset of ferroptosis in *db/db* mice was therefore assessed. The results showed that the expression of GPX4 and SLC7A11 was significantly higher in the *db/db* + AAV tRF3-IleAAT group than in the *db/db* + AAV tRF-NC group, while the expression of ACSL4 was significantly lower (Fig. 4a, b and Supplementary Fig. S4a). GSH levels were significantly elevated in the *db/db* + AAV tRF3-IleAAT group (Fig. 4c). In vitro, tRF3-IleAAT was first overexpressed in HG-induced mesangial cells, and RT-qPCR and Western blotting were performed to measure the expression levels of ferroptosis-related indicators. The results showed that the expression was significantly changed in the HG + tRF3-IleAAT mimetic group than in the HG + tRF3-IleAAT NC group (Fig. 4d, e and Supplementary Fig. S4b). ROS levels were reduced to some extent in the HG + tRF3-IleAAT group (Fig. 4f). Mitochondrial morphology was examined by transmission electron microscopy. Typical changes in mitochondria, including morphological miniaturization, increased membrane density and reduced cristae, were observed by transmission electron microscopy in the HG group. After treatment with the tRF3-IleAAT mimetic, the mitochondrial ridges of mesangial cells became clearly visible, and morphological changes such as atrophy and increased membrane density were alleviated (Fig. 4g). The results of GSH measurement showed that the GSH levels were significantly higher in the HG + tRF3-IleAAT mimetic group than in the HG + tRF3-IleAAT NC group (Fig. 4h), while the levels of  $\text{Fe}^{2+}$  and MDA tended to be lower (Fig. 4i, j), further confirming the inhibitory effect of tRF3-IleAAT on ferroptosis in DKD models.

**Knockdown of the tRF3-IleAAT downstream target gene ZNF281 alleviates ferroptosis in HG-induced mesangial cells**  
The possible mechanism by which tRF3-IleAAT reduces ECM synthesis and inhibits ferroptosis in DKD mice and HG-treated mesangial cells was further explored. The downstream target genes of tRF3-IleAAT were predicted using the miRDB database [27], which revealed 26 target genes; among these genes, ZNF281 exhibited the highest target gene score and is highly likely to be involved in tissue cell fibrosis and inflammation (Fig. 5a and Supplementary Table S3). We successfully detected significantly elevated expression of ZNF281 by RT-qPCR and Western blotting in *db/db* mice (Fig. 5b, c and Supplementary Fig. S5a). Immunohistochemical analysis showed high expression of ZNF281 in the kidney tissues of *db/db* mice (Fig. 5d). The same results were

obtained in HG-induced mesangial cells (Fig. 5e, f and Supplementary Fig. S5b). We hypothesized that tRF3-IleAAT might target ZNF281 and attenuate ferroptosis. To verify this, the expression of ZNF281 was knocked down in HG-treated mesangial cells using ZNF281 siRNA, and the knockdown efficiency was verified by RT-qPCR and Western blotting (Fig. 5g, h and Supplementary Fig. S5c). RT-qPCR and Western blotting were also used to measure the expression levels of related indicators to clarify the association of ZNF281 with the occurrence of ferroptosis and ECM synthesis. The results showed that the expression of ACSL4, FN and Col I was significantly reduced and that the expression of GPX4 and SLC7A11 was significantly elevated in the HG + ZNF281 siRNA group, as shown in Fig. 5g, h and Supplementary Fig. S5c. The GSH assays showed that the GSH levels were higher in the HG + ZNF281 siRNA group (Fig. 5i). The same result was observed in the MDA content assay (Fig. 5j), further elucidating the correlation between ZNF281 and ferroptosis.

**tRF3-IleAAT directly targets ZNF281 and negatively regulates its expression**

To further clarify the interaction between tRF3-IleAAT and the target gene ZNF281, we examined the changes in ZNF281 expression after overexpressing tRF3-IleAAT in DKD models to assess the effect of tRF3-IleAAT on gene expression levels. RT-qPCR and Western blotting results showed that the expression of ZNF281 was significantly lower in the *db/db* + AAV tRF3-IleAAT group than in the NC group (Fig. 6a, b and Supplementary Fig. S6a). Immunohistochemical analysis showed that ZNF281 expression was reduced in kidney tissues of mice in the *db/db* + tRF3-IleAAT mimetic group (Fig. 6c). After overexpressing tRF3-IleAAT in HG-treated mesangial cells, we observed the same results as in the in vivo experiments (Fig. 6d, e and Supplementary Fig. S6b). In combination with the results of previous bioinformatics analysis, these results indicated that ZNF281 is a potent downstream target of tRF3-IleAAT. There is full base complementarity between tRF3-IleAAT and the 3'UTR of ZNF281, and the sequence is conserved, as shown in Fig. 6f. To confirm the targeted binding of tRF3-IleAAT to the 3'UTR of the ZNF281 gene, reporter plasmids for the ZNF281-3'UTR-WT and ZNF281-3'UTR-MUT were constructed by RiboBio and transfected into HEK-293T cells. These plasmids were validated with a dual-luciferase reporter assay. The results showed that the luciferase activity of the tRF3-IleAAT mimetic and ZNF281-3'UTR-WT plasmids was significantly lower compared to the transfected NC (tRF3-IleAAT mimetic NC); in contrast, cotransfection of the tRF3-IleAAT mimetic and ZNF281-3'UTR-MUT plasmids did not significantly change the luciferase activity in the cells (Fig. 6g). In addition, after verifying the relationship between ZNF281 and ferroptosis, we determined whether overexpression of ZNF281 could counteract the protective effect of tRF3-IleAAT against ferroptosis and ECM synthesis in mesangial cells. We discovered that cotransfection of tRF3-IleAAT mimetic and ZNF281 plasmids largely counteracted the inhibitory effect of tRF3-IleAAT on ferroptosis and ECM synthesis, as evidenced by the significant alterations in the levels of GPX4, SLC7A11, ACSL4, FN and Col I (Fig. 6h, i and Supplementary Fig. S6c). The obtained data indicate that tRF3-IleAAT may inhibit ferroptosis and ECM synthesis by directly targeting ZNF281 in DKD.

## DISCUSSION

DKD is a progressive disease that occurs in 40% of people with diabetes [1]. There is continuous pressure to determine the pathogenesis of DKD and develop new targeted therapies [28]. Efficient DKD biomarkers are greatly needed to improve treatment. tRFs have shown great potential as a novel class of regulatory noncoding RNAs that occur widely in various organisms, and several



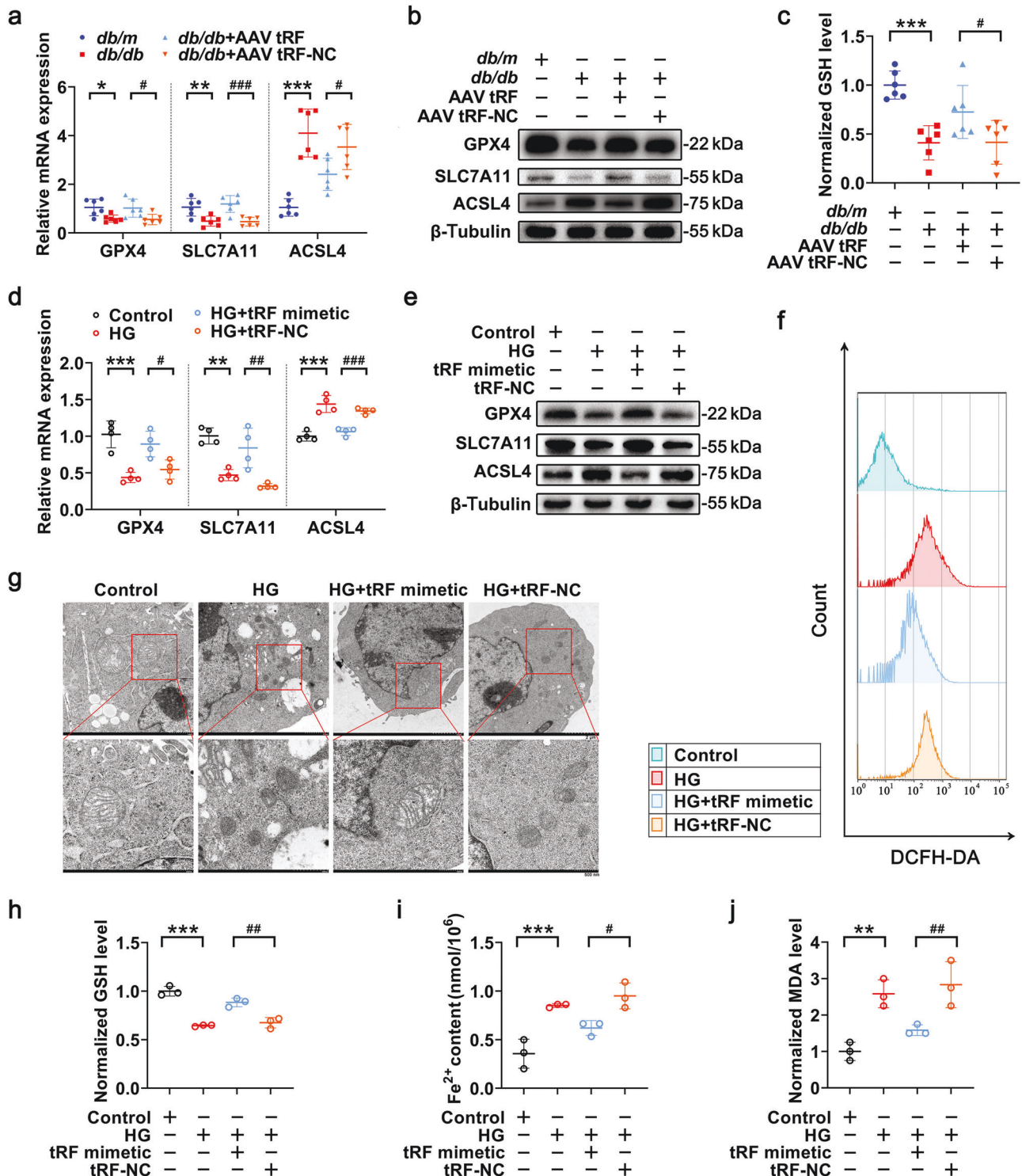


**Fig. 4** tRF3-IleAAT overexpression alleviates ferroptosis in DKD models. **a, b** RT-qPCR and Western blot analysis of ferroptosis-related indicators were performed to evaluate the role of tRF3-IleAAT in ferroptosis in *db/db* mice. **c** GSH levels in mice. **d, e** The inhibitory effect of tRF3-IleAAT on ferroptosis in HG-treated mesangial cells was demonstrated by RT-qPCR and Western blotting. **f** ROS levels were assessed by flow cytometry. **g** Transmission electron microscopy revealed mitigated mitochondrial changes after tRF3-IleAAT treatment. Furthermore, the cellular GSH levels (**h**),  $Fe^{2+}$  contents (**i**), and MDA concentrations (**j**) verified the role of tRF3-IleAAT in ferroptosis. The data are expressed as the mean  $\pm$  SD. \* $P < 0.05$ , \*\* $P < 0.01$ , \*\*\* $P < 0.001$ , # $P < 0.05$ , ## $P < 0.01$ , ### $P < 0.001$  vs. the indicated group.

studies supported by next-generation sequencing technologies have identified multiple tRFs with key roles in the development of renal diseases [15–17, 29, 30]. Our team collected clinical sera samples for screening of differentially expressed tRFs in diabetes

and DKD patients in a previous study, which was innovative in origin. The expression profiles of tRFs in DKD are available in the National Center for Biotechnology Information [ID 916973-BioProject-NCBI (nih.gov)]. The results showed a total of 6



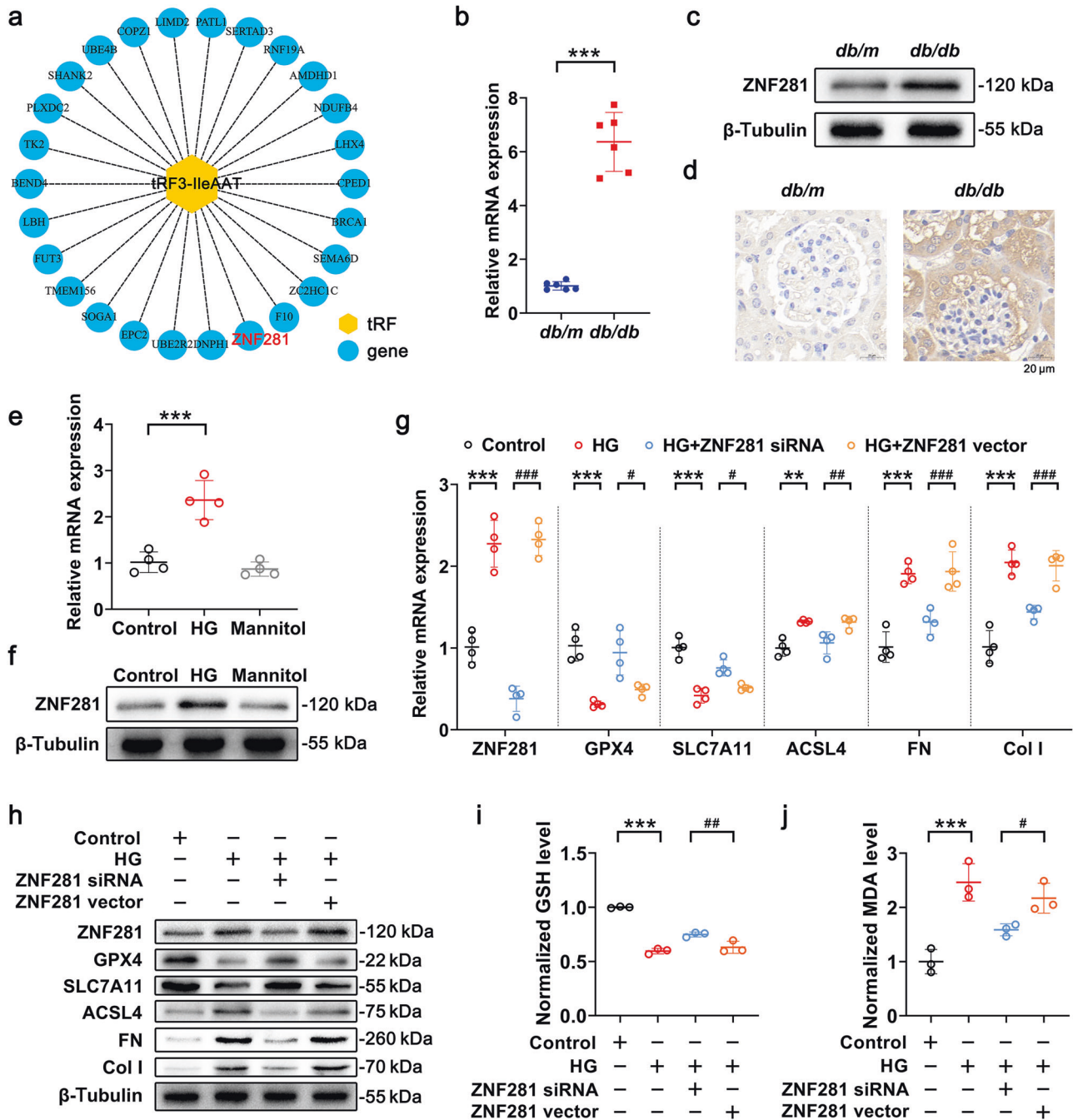


**Fig. 5** Knockdown of the tRF3-IleAAT downstream target gene ZNF281 alleviates ferroptosis in HG-induced mesangial cells. **a** Prediction of downstream target genes of tRF3-IleAAT. **b, c** RT-qPCR and Western blot analysis of ZNF281 were performed to verify its expression in *db/db* mice. **d** Immunohistochemistry was used to determine the localization and expression of ZNF281 in renal tissues. **e, f** The high expression of ZNF281 in HG-treated mesangial cells was verified. **g, h** RT-qPCR and Western blotting were used to verify the knockdown of ZNF281 in cells. The relationship between ZNF281 and ferroptosis and ECM synthesis was assessed by RT-qPCR and Western blot analysis of related indicators, and the results were further corroborated by measurement of GSH levels (**i**) and MDA contents (**j**). The data are expressed as the mean  $\pm$  SD. \*\* $P < 0.01$ , \*\*\* $P < 0.001$ , # $P < 0.05$ , ## $P < 0.01$ , ### $P < 0.001$  vs. the indicated group.

differentially expressed tRFs in serum samples, which were verified by RT-qPCR [17]. At the initial stage of this study, we performed pre-experiments in a DKD cell model and selected tRF3-IleAAT, a significantly low-expressed tRF, for further in-depth study. In previous functional analysis, enrichment of cell death and metabolism attracted our attention, and they were further found to be associated with ferroptosis-related signaling pathways, such as mammalian target of rapamycin, erythroblastic oncogene B and adenosine 5'-monophosphate-activated protein kinase. Here,

ferroptosis was used as an entry point to delve into the pathways and mechanisms by which tRF3-IleAAT regulates ECM synthesis in DKD. tRFs have not been studied much in the field of renal disease, and tRF3-IleAAT has not been reported yet, especially in relation to its interaction with ferroptosis. We innovatively explored the role and mechanism of tRF3-IleAAT in DKD, which provide a new target for intervention in the diagnosis and treatment of DKD.

Ferroptosis, a unique form of cell death, is involved in regulating the development of multiple systemic diseases. Iron homeostasis

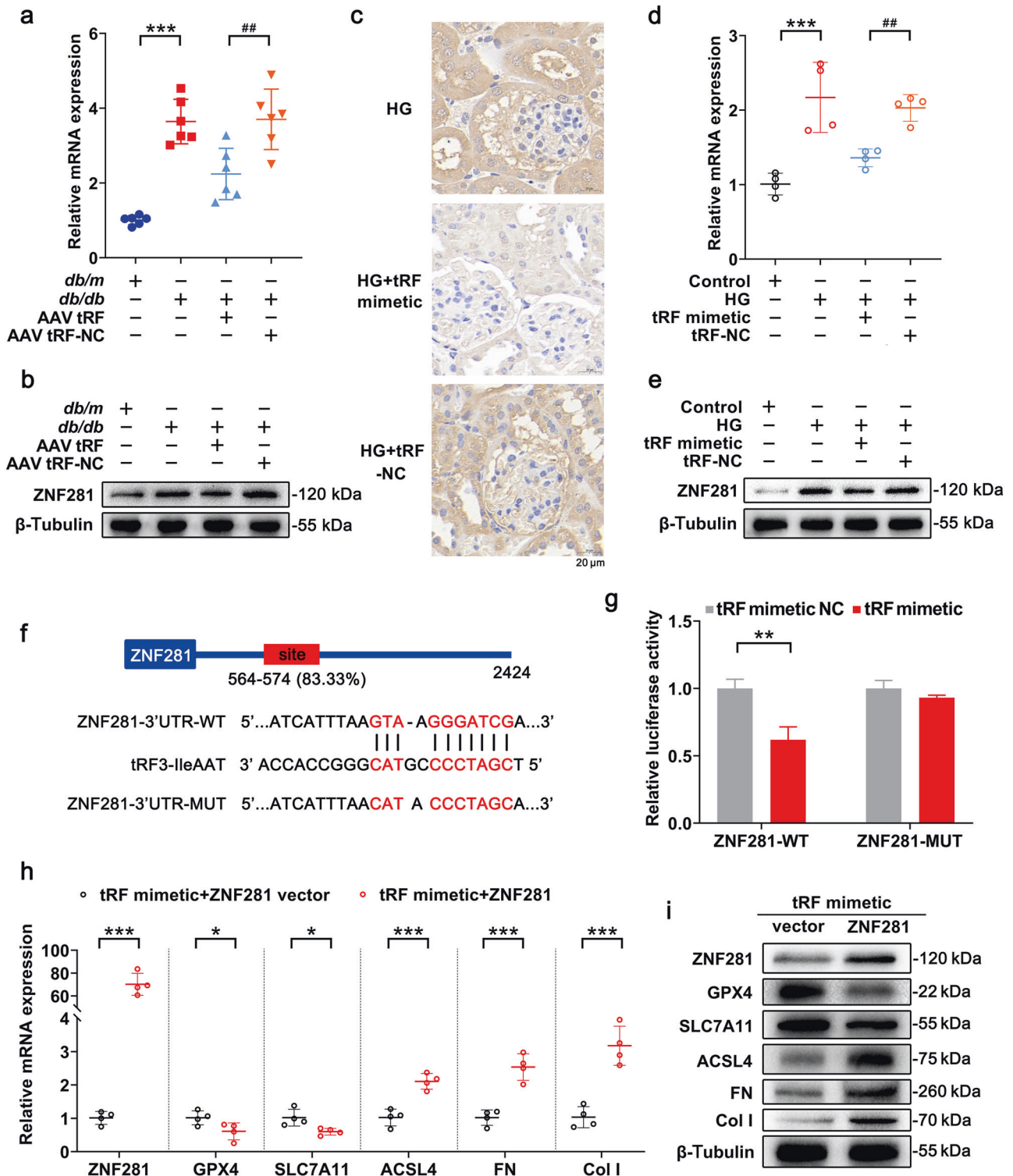


**Fig. 6** tRF3-IleAAT directly targets ZNF281 and negatively regulates its expression. **a, b** RT-qPCR and Western blotting were used to examine the expression of ZNF281 after tRF3-IleAAT overexpression in *db/db* mice. **c** Immunohistochemistry was used to determine the expression of ZNF281 in renal tissues. **d, e** The expression of ZNF281 after tRF3-IleAAT overexpression in HG-induced mesangial cells was measured through RT-qPCR and Western blotting. **f** The predicted binding site between the 3'UTR of ZNF281 mRNA and tRF3-IleAAT. **g** Dual-luciferase reporter assay showing the difference in fluorescence activity after each subgroup was cotransfected. **h, i** RT-qPCR and Western blotting were used to assess the expression levels of ZNF281 and ferroptosis-related indicators after cotransfection of tRF3-IleAAT mimetic and ZNF281 plasmids in mesangial cells. The data are expressed as the mean  $\pm$  SD. \* $P$  < 0.05, \*\* $P$  < 0.01, \*\*\* $P$  < 0.001, ## $P$  < 0.01 vs. the indicated group.

determines the normal function of renal cells, and CKD is also closely associated with oxidative stress and mitochondrial dysfunction [31, 32]. Growing evidence has shown that ferroptosis plays a crucial role in renal diseases [22–24, 33–35], providing new opportunities for the diagnosis and management of DKD. Since the initial description of ferroptosis, an increasing number of genes or proteins that are involved in this cell death process have been identified [36]. GPX4 reduces intracellular lipid peroxidation [19], and SLC7A11 promotes GSH production by translocating cysteine into the cytoplasm, thus reducing cellular lipid peroxidation levels to inhibit ferroptosis [37]; these are classical pathways regulating ferroptosis. The interactions between ferroptosis and noncoding RNAs are also attracting attention; for example, the potential involvement of noncoding RNAs, which induce ferroptosis in acute kidney injury by inducing the upregulation of microRNA-182-5p and microRNA-378-3p expression, has been demonstrated in acute injury models [38]. The link between ferroptosis and tRFs has been poorly studied, but a recent study reported that the alveolar macrophage-derived exosome tRF-22-8BWS7K092 can induce ferroptosis in acute lung injury by activating the Hippo signaling pathway [39]. Studies on the role and mechanism of tRFs in ferroptosis are rare, especially in the field of DKD. We innovatively propose that tRF3-IleAAT, a tRF whose expression is reduced in the sera of patients with DKD, inhibits ferroptosis and thus reduces ECM synthesis in DKD mesangial cells.

Here, we found reduced tRF3-IleAAT expression and increased ECM synthesis in *db/db* mice and HG-treated mesangial cells, and we detected ferroptosis along with a significant decrease in renal function in *db/db* mice. We observed that tRF3-IleAAT overexpression in DKD models inhibited ferroptosis, reduced ECM synthesis, and alleviated renal dysfunction in *db/db* mice, suggesting that tRF3-IleAAT participates in the regulation of ferroptosis and fibrosis in DKD. Fer-1, a classical ferroptosis inhibitor, was used in DKD models. To further investigate the critical role of ferroptosis in ECM synthesis in renal fibrosis, we performed ferroptosis inhibition experiments and verified the interference efficiency. The experiments demonstrated that ferroptosis in *db/db* mice and HG-induced mesangial cells was effectively inhibited by Fer-1; in addition, renal fibrosis was further alleviated, and ECM and collagen deposition were reduced in DKD models, confirming the vital role of ferroptosis in the progression of DKD. Given these findings, we preliminarily concluded that tRF3-IleAAT reduces the synthesis of ECM in DKD mesangial cells through the inhibition of ferroptosis.

We further explored the potential mechanism by which tRF3-IleAAT inhibits the onset of ferroptosis in DKD. tRF utilizes a mode of action similar to that of microRNAs, including binding to target genes. Through bioinformatics analysis and expression level validation, we obtained evidence that ZNF281 is a dominant downstream target gene. Zinc finger proteins are members of a class of transcription factors containing finger-like structural domains that bind to GC-enriched regions in the promoters of a variety of genes. These proteins play critical roles in gene regulation, are key regulators of tissue development [40] and are significantly upregulated in human malignancies, including colon and kidney cancers [41–44]. ZNF281 has now been investigated and identified as an epithelial-mesenchymal transition-inducible transcription factor [42]. Silencing ZNF281 in inflammatory bowel disease significantly reduces the expression of inflammatory factors and fibrosis genes and abolishes the elevations in extracellular collagen levels and morphological changes induced by inflammation [45]. We detected significantly elevated expression of ZNF281 in DKD models, suggesting that ZNF281 may also be associated with renal fibrosis in DKD, while its relationship with ferroptosis has not been previously reported. As ZNF281 is a downstream target gene of tRF3-IleAAT, we used ZNF281 as an entry point to thoroughly investigate the potential

mechanisms by which tRF3-IleAAT inhibits the onset of ferroptosis in DKD. After knocking down the expression of ZNF281 in HG-treated mesangial cells, we found that ferroptosis was significantly inhibited. Upon overexpression of tRF3-IleAAT, a significant reduction in the expression level of ZNF281 was detected, and the targeted binding of tRF3-IleAAT to the ZNF281 3'UTR was further validated by a dual-luciferase reporter assay. Cotransfection of tRF3-IleAAT mimetic and ZNF281 plasmids largely counteracted the inhibitory effect of tRF3-IleAAT on ferroptosis. Our data suggest that tRF3-IleAAT inhibits ferroptosis by reducing the expression of ZNF281 in HG-induced mesangial cells.

In summary, this study illustrates the role and mechanism of tRF3-IleAAT in a DKD animal model and HG-treated mesangial cells. We propose that tRF3-IleAAT inhibits ferroptosis by decreasing the expression of ZNF281 to reduce ECM synthesis in mesangial cells and delay the progression of DKD. However, the mechanism of the role of zinc finger proteins in ferroptosis deserves further in-depth subsequent investigation. In addition, we expect to be able to determine the manner in which ZNF281 regulates the development of DKD in animal models in subsequent studies. This study provides new insights into the molecular mechanism of DKD from the perspective of tRFs and ferroptosis and contributes to a theoretical basis for the clinical diagnosis and treatment of DKD.

## ACKNOWLEDGEMENTS

This study was supported by the National Natural Science Foundation of China (No. 81970664), the Natural Science Foundation of Jiangsu Province (Nos. BK20211385 and BK20191082), the Dedicated Fund for Pediatric Medical Research of Jiangsu Province Medical Association (Nos. SYH-32034-0073 and SYH-32034-0085), and the 789 Outstanding Talent Program of SAHNMU (No. 789ZYRC202090251). We are grateful to the experimental center of the Second Affiliated Hospital of Nanjing Medical University for providing the platform.

## AUTHOR CONTRIBUTIONS

AQZ and HMS conceived and designed the experiments. YYQ, JLJ and WLH performed the experiments and analysed the data. YYQ wrote the manuscript. JLJ helped edit the manuscript, and WLH drew graphic materials. AQZ and HMS revised the manuscript and confirmed the authenticity of all the raw data. GTQ, SWL, XYL, RJ and YFL contributed to the data analysis and graphical abstract. All authors have read and endorsed the final manuscript.

## ADDITIONAL INFORMATION

**Supplementary information** The online version contains supplementary material available at <https://doi.org/10.1038/s41401-024-01228-5>.

**Competing interests:** The authors declare no competing interests.

## REFERENCES

1. Alicic RZ, Rooney MT, Tuttle KR. Diabetic kidney disease: challenges, progress, and possibilities. *Clin J Am Soc Nephrol*. 2017;12:2032–45.
2. Thurlow JS, Joshi M, Yan G, Norris KC, Agodoa LY, Yuan CM, et al. Global epidemiology of end-stage kidney disease and disparities in kidney replacement therapy. *Am J Nephrol*. 2021;52:98–107.
3. Calle P, Hotter G. Macrophage phenotype and fibrosis in diabetic nephropathy. *Int J Mol Sci*. 2020;21:2806.
4. Humphreys BD. Mechanisms of renal fibrosis. *Annu Rev Physiol*. 2018;80:309–26.
5. Tonneijck L, Muskiet MH, Smits MM, van Bommel EJ, Heerspink HJ, van Raalte DH, et al. Glomerular hyperfiltration in diabetes: mechanisms, clinical significance, and treatment. *J Am Soc Nephrol*. 2017;28:1023–39.
6. Zhao JH. Mesangial cells and renal fibrosis. *Adv Exp Med Biol*. 2019;1165:165–94.
7. Jiang S, Su H. Cellular crosstalk of mesangial cells and tubular epithelial cells in diabetic kidney disease. *Cell Commun Signal*. 2023;21:288.
8. Thomas HY, Ford Versypt AN. Pathophysiology of mesangial expansion in diabetic nephropathy: mesangial structure, glomerular biomechanics, and biochemical signaling and regulation. *J Biol Eng*. 2022;16:19.
9. Thompson DM, Parker R. Stressing out over tRNA cleavage. *Cell*. 2009;138:215–9.



10. Li NS, Shan NY, Lu LG, Wang ZH. tRFtarget: a database for transfer RNA-derived fragment targets. *Nucleic Acids Res.* 2021;49:D254–D260.
11. Xie YY, Yao LP, Yu XC, Ruan Y, Li Z, Guo JM. Action mechanisms and research methods of tRNA-derived small RNAs. *Signal Transduct Target Ther.* 2020;5:109.
12. Yu XC, Xie YY, Zhang SS, Song XM, Xiao BX, Yan ZL. tRNA-derived fragments: mechanisms underlying their regulation of gene expression and potential applications as therapeutic targets in cancers and virus infections. *Theranostics.* 2021;11:461–9.
13. Fagan SG, Helm M, Prehn JHM. tRNA-derived fragments: a new class of non-coding RNA with key roles in nervous system function and dysfunction. *Prog Neurobiol.* 2021;205:102118.
14. Zhou JH, Liu SX, Chen Y, Fu Y, Silver AJ, Hill MS, et al. Identification of two novel functional tRNA-derived fragments induced in response to respiratory syncytial virus infection. *J Gen Virol.* 2017;98:1600–10.
15. Lu XY, Zhu XY, Yu MY, Na C, Gan WH, Zhang AQ. Profile analysis reveals transfer RNA fragments involved in mesangial cells proliferation. *Biochem Biophys Res Commun.* 2019;514:1101–7.
16. Shi HM, Yu MY, Wu Y, Cao YP, Li SW, Qu GT, et al. tRNA-derived fragments (tRFs) contribute to podocyte differentiation. *Biochem Biophys Res Commun.* 2020;521:1–8.
17. Huang C, Ding L, Ji JL, Qiao YY, Xia ZH, Shi HM, et al. Expression profiles and potential roles of serum tRNA-derived fragments in diabetic nephropathy. *Exp Ther Med.* 2023;26:311.
18. Dixon SJ, Lemberg KM, Lamprecht MR, Skouta R, Zaitsev EM, Gleason CE, et al. Ferroptosis: an iron-dependent form of nonapoptotic cell death. *Cell.* 2012;149:1060–72.
19. Yang WS, SriRamaratnam R, Welsch ME, Shimada K, Skouta R, Viswanathan VS, et al. Regulation of ferroptotic cancer cell death by GPX4. *Cell.* 2014;156:317–31.
20. Wang LY, Liu YC, Du TT, Yang H, Lei L, Guo MQ, et al. ATF3 promotes erastin-induced ferroptosis by suppressing system Xc. *Cell Death Differ.* 2020;27:662–75.
21. Chen X, Li JB, Kang R, Klionsky DJ, Tang DL. Ferroptosis: machinery and regulation. *Autophagy.* 2021;17:2054–81.
22. Martin-Sanchez D, Ruiz-Andres O, Poveda J, Carrasco S, Cannata-Ortiz P, Sanchez-Niño MD, et al. Ferroptosis, but not necroptosis, is important in nephrotoxic folic acid-induced AKI. *J Am Soc Nephrol.* 2017;28:218–29.
23. Li SW, Zheng LS, Zhang J, Liu XJ, Wu ZM. Inhibition of ferroptosis by up-regulating Nrf2 delayed the progression of diabetic nephropathy. *Free Radic Biol Med.* 2021;162:435–49.
24. Wang JY, Wang YQ, Liu Y, Cai XT, Huang X, Fu WJ, et al. Ferroptosis, a new target for treatment of renal injury and fibrosis in a 5/6 nephrectomy-induced CKD rat model. *Cell Death Discov.* 2022;8:127.
25. Sharma K, McCue P, Dunn SR. Diabetic kidney disease in the *db/db* mouse. *Am J Physiol Ren Physiol.* 2003;284:F1138–F1144.
26. Miotto G, Rossetto M, Di Paolo ML, Orian L, Venerando R, Roveri A, et al. Insight into the mechanism of ferroptosis inhibition by ferrostatin-1. *Redox Biol.* 2020;28:101328.
27. Liu WJ, Wang XW. Prediction of functional microRNA targets by integrative modeling of microRNA binding and target expression data. *Genome Biol.* 2019;20:18.
28. Tuttle KR, Agarwal R, Alpers CE, Bakris GL, Brosius FC, Kolkhof P, et al. Molecular mechanisms and therapeutic targets for diabetic kidney disease. *Kidney Int.* 2022;102:248–60.
29. Li SW, Liu YW, He XW, Luo XG, Shi HM, Qu GT, et al. tRNA-derived fragments in podocytes with adriamycin-induced injury reveal the potential mechanism of idiopathic nephrotic syndrome. *Biomed Res Int.* 2020;2020:7826763.
30. Li D, Zhang H, Wu XQ, Dai Q, Tang SQ, Liu Y, et al. Role of tRNA derived fragments in renal ischemia-reperfusion injury. *Ren Fail.* 2022;44:815–25.
31. Ho HJ, Shirakawa H. Oxidative stress and mitochondrial dysfunction in chronic kidney disease. *Cells.* 2022;12:88.
32. Jha JC, Banal C, Chow BS, Cooper ME, Jandeleit-Dahm K. Diabetes and kidney disease: role of oxidative stress. *Antioxid Redox Signal.* 2016;25:657–84.
33. Wang JY, Liu Y, Wang YQ, Sun L. The cross-link between ferroptosis and kidney diseases. *Oxid Med Cell Longev.* 2021;2021:6654887.
34. Zhang XQ, Li XG. Abnormal iron and lipid metabolism mediated ferroptosis in kidney diseases and its therapeutic potential. *Metabolites.* 2022;12:58.
35. Wu Y, Zhao Y, Yang HZ, Wang YJ, Chen Y. HMGB1 regulates ferroptosis through Nrf2 pathway in mesangial cells in response to high glucose. *Biosci Rep.* 2021;41:BSR20202924.
36. Sheng XH, Shan C, Liu JB, Yang JT, Sun B, Chen DZ. Theoretical insights into the mechanism of ferroptosis suppression via inactivation of a lipid peroxide radical by liproxstatin-1. *Phys Chem Chem Phys.* 2017;19:13153–9.
37. Fang XX, Cai ZX, Wang H, Han D, Cheng Q, Zhang P, et al. Loss of cardiac ferritin h facilitates cardiomyopathy via slc7a11-mediated ferroptosis. *Circ Res.* 2020;127:486–501.
38. Ding CG, Ding XM, Zheng J, Wang B, Li Y, Xiang HL, et al. miR-182-5p and miR-378a-3p regulate ferroptosis in I/R-induced renal injury. *Cell Death Dis.* 2020;11:929.
39. Wang WX, Zhu L, Li HT, Ren WY, Zhuo R, Feng CC, et al. Alveolar macrophage-derived exosomal tRF-22-8BWS7K092 activates Hippo signaling pathway to induce ferroptosis in acute lung injury. *Int Immunopharmacol.* 2022;107:108690.
40. Fidalgo M, Shekar PC, Ang YS, Fujiwara Y, Orkin SH, Wang J. Zfp281 functions as a transcriptional repressor for pluripotency of mouse embryonic stem cells. *Stem Cells.* 2011;29:1705–16.
41. Deng YR, Peng DZ, Xiao J, Zhao YH, Ding WH, Yuan ST, et al. Inhibition of the transcription factor ZNF281 by SUFU to suppress tumor cell migration. *Cell Death Differ.* 2023;30:702–15.
42. Hahn S, Hermeking H. ZNF281/ZBP-99: a new player in epithelial-mesenchymal transition, stemness, and cancer. *J Mol Med.* 2014;92:571–81.
43. Qin CJ, Bu PL, Zhang Q, Chen JT, Li QY, Liu JT, et al. ZNF281 regulates cell proliferation, migration and invasion in colorectal cancer through wnt/ $\beta$ -catenin signaling. *Cell Physiol Biochem.* 2019;52:1503–16.
44. Laudadio I, Bastianelli A, Fulci V, Carissimi C, Colantoni E, Palone F, et al. ZNF281 promotes colon fibroblast activation in TGF $\beta$ 1-induced gut fibrosis. *Int J Mol Sci.* 2022;23:10261.
45. Pierdomenico M, Palone F, Cesi V, Vitali R, Mancuso AB, Cucchiara S, et al. Transcription factor ZNF281: a novel player in intestinal inflammation and fibrosis. *Front Immunol.* 2018;9:2907.

Springer Nature or its licensor (e.g. a society or other partner) holds exclusive rights to this article under a publishing agreement with the author(s) or other rightsholder(s); author self-archiving of the accepted manuscript version of this article is solely governed by the terms of such publishing agreement and applicable law.